Incremental Step Reference Governor for Load Conditioning of Hybrid Fuel Cell and Gas Turbine Power Plants

Vasilis Tsourapas, Jing Sun, *Fellow, IEEE*, and Anna Stefanopoulou

***Abstract*—A hybrid solid oxide fuel cell and gas turbine (SOFC/GT) system exploits the complementary features of the two power plants, where the GT recuperates the energy in the SOFC exhaust stream and thereby boosting the overall system efficiency. Through model based transient analysis, however, it is shown that the intricate coupling dynamics make the transient load following very challenging. Power shutdown has been observed when the load is changed abruptly in the generator. In this work, a novel closed-loop reference governor controller is proposed to mitigate the shutdown phenomenon. The reference governor utilizes the region of attraction of a reduced order SOFC/GT model to determine if an incremental step change is allowable, i.e., it does not cause a shutdown. It is shown that with a moderate computational cost, the speed of the hybrid power system response can be improved significantly compared to the fastest conventional load filter. Several design parameters, such as the sampling rate and incremental step-size, are also explored to understand the trade-offs between computational complexity and performance improvement.**

***Index Terms*—Dynamics, feedback control, fuel cells (FCs), hybrid, modeling, solid oxide fuel cell (SOFC).**

NOMENCLATURE

Symbols

$c_{(\cdot)}$	Concentration of species $(\cdot)$ (mole).
c_P	Heat capacity (J/kgK).
H^{abs}	Absolute enthalpy (J/kg).
i	Current density (A/m^2).
I_{st}	Stack current–input (A).
J	Shaft inertia (kgm^2).
m	Mass (kg).
M	Molar Weight (kg/mole).
N	Shaft rotational speed (r/min).
$p_{(\cdot)}$	Pressure of $(\cdot)$ (Pa).
P	Power (W).
R_A	Region of attraction.
T	Temperature (K).
U	Voltage (V).
u_{rg}	Reference governor command.
V	Volume (m^3).
W	Flow (kg/s).
$x_{(\cdot)}$	Molar fraction of species $(\cdot)$.

Abbreviations

C	Compressor.
CB	Catalytic burner.
ERD	Energy recuperation device.
FC	Fuel cell.
FOM	Full order model.
GEN	Generator.
GT	Gas Turbine.
IS-RG	Incremental step reference governor.
RG	Reference governor.
ROM	Reduced order model.
SOFC	Solid oxide fuel cell.
T	Turbine.

Manuscript received May 04, 2008; revised August 22, 2008. Manuscript received in final form November 06, 2008. First published April 17, 2009; current version published June 24, 2009. Recommended by Associate Editor N. Kazantzis. This work was supported in part by the ONR under Contract N00014-06-1-0209 and NSF ECS-0501284.

V. Tsourapas is with Eaton Corporation, Innovation Center, Southfield, MI 48076 USA (e-mail: vasiliostsourapas@eaton.com).

J. Sun is with the Department of Naval Architecture and Marine Engineering, University of Michigan, Ann Arbor, MI 48109-2145 USA (e-mail: jingsun@umich.edu).

A. Stefanopoulou is with the Department of Mechanical Engineering, University of Michigan, Ann Arbor, MI 48109-2121 USA (e-mail: annastef@umich.edu).

Color versions of one or more of the figures in this paper are available online at http://ieeexplore.ieee.org.

Digital Object Identifier 10.1109/TCST.2008.2010554

I. INTRODUCTION

FUEL cell (FC)-based power plants offer high efficiency and low emissions compared to conventional power production technologies such as diesel or gasoline engines. Integrating fuel cell based power systems with energy recuperation devices (ERDs) can further improve the system efficiency by reducing the exhaust energy losses. Such integration often results in hybrid power systems, of which the combination of the

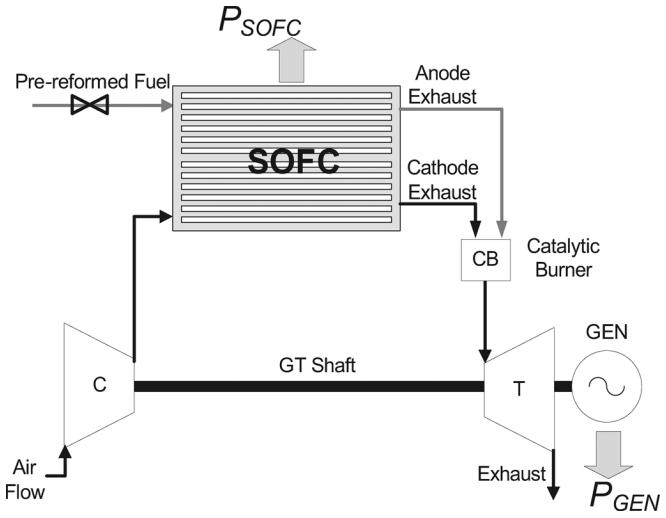

Fig. 1. Hybrid SOFC/GT configuration.

solid oxide fuel cell (SOFC) and gas turbine (GT) studied in this paper is a representative configuration (see Fig. 1).

Energy recuperation is critical in achieving high system efficiency and in assuring minimal energy losses to the environment. FC systems are ideal candidates for incorporating energy recuperation devices for several reasons. In order to assure high efficiency and to avoid hydrogen starvation,[1] fuel cell stacks do not operate at fuel utilization ratios close to 100% [1], [2]. The existence of the unused fuel in the exhaust represents a significant opportunity for energy recovery. For the high temperature SOFCs, especially for the pressurized SOFCs, the high exhaust temperature and energy content make the energy recuperation even more attractive. The main devices used to facilitate energy recuperation from SOFC systems are catalytic burner (CB) and gas turbine (GT) combinations as shown in Fig. 1.

The integrated fuel cell systems with energy recuperation devices have been studied extensively in the literature, motivated by the substantial benefits of ERDs. Several studies show that the steady state efficiency increases when energy recuperation devices are incorporated in a fuel cell system [3], [4]. Other publications on control oriented analysis of FC systems identify the load following limitations and implement model predictive control schemes to resolve them [5]–[7]. On coupled SOFC/GT systems, a dynamic model of an SOFC/GT system is developed in [8]. The model is validated using experimental data provided by Siemens Westinghouse and the authors note that the model, built from first principles, can reasonably predict the dynamic performance of a complex hybrid FC/GT system. The authors of [9] develop a dynamic model of an SOFC/GT system and evaluate the matching between that model and a linearized version of the same model. They note that the linear and nonlinear model responses match only for small range of variations (less that 10%) in the inputs. Thus, the nonlinearities cannot be ignored in the performance analysis. In [10], using dynamic analysis, it is identified that regulating the shaft speed in an SOFC/GT system can be achieved by direct injection of fuel flow in the catalytic burner. Finally, Stiller *et al.* [10] pointed out that:

> With a given constant generator power, the system is at an unstable equilibrium. Departing from steady-state, for example, a step increase of the generator power will lead to deceleration of the shaft speed. No new equilibrium will be found within the valid bounds of shaft speed.

The authors note that proper shaft speed regulation can be achieved via trial-and-error tuning of a PID controller, using as feedback the error between the actual air flow and the air flow setpoint. The system stability, though, is not guaranteed for a load step different from the one the PID controller was tuned for.

The focus of this paper is on achieving efficient steady-state operation and fast transient response for a highly coupled SOFC and gas turbine system. The contribution of the paper, besides the development of a control oriented system model and model-based dynamic analysis, is the design and implementation of a load governor scheme to safeguard the system during transient operation. The proposed algorithm avoids online optimization, which often incurs significant computational cost, by leveraging the knowledge of the system dynamics.

This paper is organized as follows. The system is described in Section II, while the system efficiency optimization along with its open loop analysis is presented in Section III. Load following limitations of the system are identified in the same section and potential solutions to mitigate them are proposed. The performance achieved by a rate limiter load conditioning system is also shown in Section III. In Section IV, the incremental step reference governor (IS-RG) is developed and integrated into the system to ensure proper load following capabilities. A detailed reduced-order model is used to develop a characterization of the region of attraction, and this model is described together with IS-RG implementation scheme in Section IV. Finally, the benefits of combining the IS-RG with a proportional feedback control is shown through simulation in Section V, before concluding with remarks in Section VI.

II. System Operation Principle

The hybrid SOFC/GT system analyzed in this work is intended as an auxiliary power unit (APU) for military and commercial applications. It is rated at 30 kW and the key components include a compressor (C), an SOFC stack, a catalytic burner (CB), and a turbine (T) which drives a generator (GEN) as shown in Fig. 1. Other components, such as the reformer and the heat exchangers, are not included in this work in order to focus on the coupling dynamics between the SOFC and the GT. While we believe that the omission of other balance-of-plant components, such as the heat exchangers, does not change the nature of the coupling dynamics between the SOFC and GT, the quantitative effects of temperature coupling introduced by the heat exchangers will be the subject of our future work. The addition of a fuel reformer, on the other hand, will affect the fuel dynamics. In this work, however, we assume that fast fuel delivery is achieved via an accumulator or a tank for pre-reformed fuel, therefore the omission of the fuel reformer does not change the nature of this study.

[1]FC hydrogen starvation is defined as the condition when less hydrogen is provided to the fuel cell than the one required for the fuel cell to produced the load drawn

The air to the SOFC is supplied to the cathode side by a compressor, while fuel is fed to the anode side. The exhaust from the SOFC outlet passes through the CB where the unused fuel is burned to increase the temperature and pressure of the flow. The high temperature and high pressure flow from the CB then powers the turbine, thereby providing a mechanism to recuperate the exhaust energy. The turbine drives both the compressor and the generator through a mechanical shaft; the former delivers the air needed for the SOFC stack operation and the latter provides additional electrical power for the system. The net power output is the sum of the electric power from the SOFC and the generator. In order to explore the dynamic characteristics of the integrated SOFC/GT system, our effort is initially devoted to developing a dynamic model that captures both the steady state and dynamic behavior of the system. The modeling details for components can be found in [1], [11] for the SOFC and in [2], [12]–[14] for the CB, GT, and the integrated system.

The integrated model has 55 states, of which 52 are the necessary states for capturing the SOFC dynamics from [1], 2 are from the CB and 1 is from the GT shaft dynamics. The main SOFC states include the temperature, flow and chemical kinetics. The input variables to the system are the fuel flow, W_f, the current drawn from the SOFC stack I_{st} and the generator load P_{gen}. The optimal setpoints for these inputs to achieve the best system efficiency are determined by an optimization, as elaborated in the next section, while a simplified model used to explain the control methodology proposed in this work is also developed in subsequent sections.

III. Open-Loop Analysis

In this section, we first perform the model-based optimization to determine the setpoints for the fuel flow, the generator load and the SOFC current. It is shown that the system is susceptible to power shutdown when an abrupt load increase is applied. The model-based analysis shows that shutdown occurs even when a small load step is applied, thereby rendering the feedforward control based on the optimized setpoints not feasible for this highly integrated system. Further analysis reveals that this phenomenon is largely attributed to the shaft rotational dynamics and the rapid increase in the generator load.

A. Steady-State Optimization

The hybrid SOFC/GT system involves multiple actuators and inputs whose setting will dictate the system operation safety and efficiency. In this study, three inputs: the fuel flow supply, the current drawn from the SOFC and the load applied to the generator, are considered. For a given fuel flow, different combinations of current drawn from the SOFC and load applied to the generator will yield different net power. Note that the net power, P_{net}, of the system is defined as the sum of the power output of the fuel cell P_{fc} and the power output of the generator P_{gen}

$$P_{\text{net}} = P_{fc} + P_{\text{gen}}. \tag{1}$$

In order to determine the maximum steady-state net power output for a given fuel flow, the following optimization problem is solved using the developed model and gradient optimization:

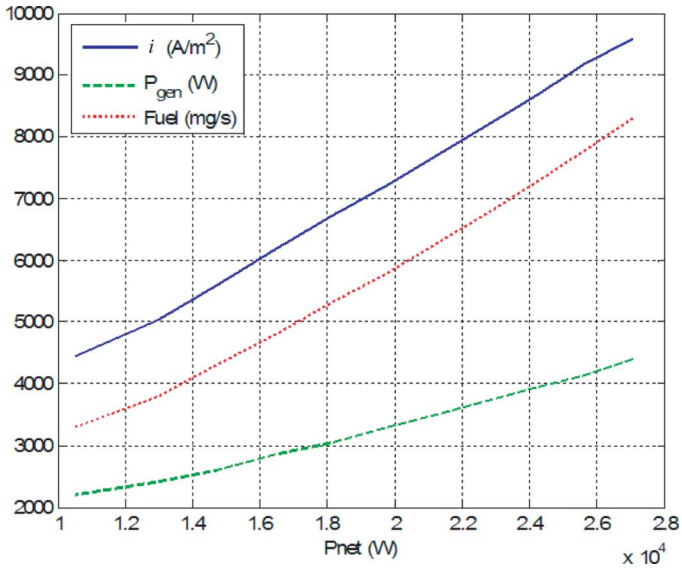

Fig. 2. Steady-state optimal setpoints (FF map) for current density (i), fuel and generator load (P^d_{gen}) as functions of net load.

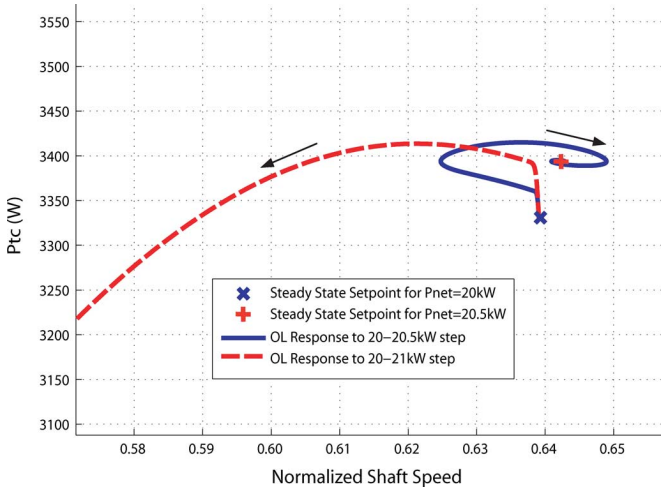

Fig. 3. System response for a 20–20.5 kW and a 20–21 kW step change in net power.

$$\max_{I_{st}, P_{\text{gen}}} (P_{\text{net}}) \text{ for given } W_f. \tag{2}$$

Note that this optimization problem yields the operating points that correspond to the optimal efficiency. By repeating the optimization problem for different fuel flows, the optimal steady-state operation setpoints are obtained as shown in Fig. 2 for the current density to be drawn from the SOFC unit,[2] the required fuel flow and the power delivered by the generator as functions of the net power generated by the integrated system. The results can be used as static feedforward maps to schedule the input variables and power split between the two power plants to achieve the maximum steady state efficiency for different power

[2]Note that $I_{st} = A_c \cdot i$, where A_c is the cell area and i is the current density (A/m^2).

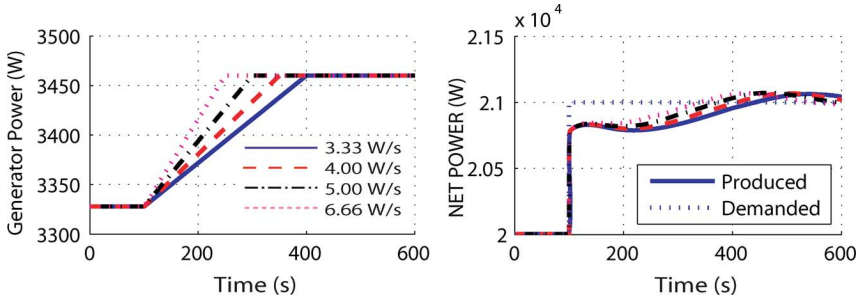

Fig. 4. Step responses from 20 to 21 kW with various rate limiters on $P_{\rm gen}$.

demands. This operation strategy, where the inputs are determined as functions of the net power demand, is referred to in this work as the open-loop control scheme.

B. Shutdown Phenomenon of the Open-Loop System

In this section, dynamic analysis is performed to understand the open-loop system dynamic characteristics. It is shown that the system is susceptible to power shutdown when an abrupt load increase is applied. The analysis here reveals that the shutdown is initiated by the gas turbine through the shaft dynamic coupling with the SOFC air supply system.

Without any feedback control in place, we consider the open loop response when a demanded load power step, from $P^d_{\rm net} =$ 20 kW to $P^d_{\rm net} = 21$ kW, is applied. The optimal input settings, identified from the optimization, are used to change the fuel flow, the current density drawn from the SOFC and the generator power from 5.8 to 6.2 g/s, 7296 to 7622 A/m^2 and 3.30 to 3.49 kW, respectively, synchronized with the change in power demand. It is observed that the system shuts down (namely, the shaft speed N goes to zero) in about 20 s after the steps are applied. For a smaller step though, from 20 to 20.5 kW, the shaft is able to support the applied load and the system reaches the desired net power after 31 seconds. The two trajectories corresponding to the two step responses are shown in Fig. 3 in the P_{tc}, N plane. Note that P_{tc} is defined as the difference between the turbine and the compressor power

$$P_{tc} = P_t \cdot \eta_m - P_c. \tag{3}$$

During the 20 to 21 kW step, the large and sudden increase (step) in the generator load deprives the compressor from having enough power to supply the air during the transient to support the SOFC operation. The sudden increase of load on the shaft first initiates a speed reduction of the shaft, which then causes a decrease in air flow to the SOFC unit that results in reduced exhaust energy out of SOFC. The decrease in the exhaust energy will cause further reduction of the shaft speed, and this positive feedback will lead the turbine shaft to stall and eventually the system to shut down. Therefore, open loop feedforward operation using the optimal steady-state setpoints without load rate limiting or load command filtering is not an option for rapid load following.

For load shedding, when a net power down step is applied, the rapid reduction of the generator load will cause a significant overshoot in air supply to the SOFC which in turn leads to a reduction in the SOFC temperature. However, due to the large SOFC thermal inertial, this temperature transient happens gradually and smoothly. Thus, no transient issues associated with load shedding are identified. More effort will be required in the future to explore the potential issues associated with rapid changes in the temperature spatial gradients that might cause material degradation.

C. Transient Response With a Rate Limiter

Given that a rapid increase in the generator load was shown to be the main cause of system shutdown, an intuitive solution is to add a rate limiter to slow down the application of $P_{\rm gen}$. Multiple rate limits are examined, varying from 3.3 to 6.7 W/s. From Fig. 4, one can see that while the system shutdown is avoided, however, the net power response will depend on the rate limit.

To understand the response shown in Fig. 4, we refer to (1). The generator load affects the net power through two paths: the direct one and the indirect one via the SOFC power

$$P_{\rm net} = P_{\rm gen} + P_{fc}(P_{\rm gen}). \tag{4}$$

The second path is mainly due to the SOFC-GT coupling. Note that lower $P_{\rm gen}$ will lead to more air being delivered to the SOFC, which results in lower SOFC temperature and thus lower SOFC power. Therefore, the power response will have double penalty when $P_{\rm gen}$ is slowed down. Another issue with a constant rate limiter is that when it is optimized for a given step, it will be suboptimal for smaller steps and insufficient for larger steps. In order to optimize the performance for all operating conditions, the limiter has to be scheduled not only for different step sizes, but also for different state conditions. This motivates us to seek for other solutions that can minimize the negative effects on power response while ensuring a safe transition.

Note that with the open loop feedforward control, the fastest rate limiter on $P_{\rm gen}$ that will not cause shutdown for a 20 to 21 kW step is 6.67 W/s. This rate limit results in a $P_{\rm net}$ settling time[3] of 168 s.

IV. Incremental Step Reference Governor

Guided by the analysis of the shutdown dynamics, we propose a load governor for the generator to throttle the load application whenever necessary to avoid shut down. While the controller is designed based on the reference governor approach found in [15], the novel aspect of this development lies in the implementation algorithm.

[3]Settling time (ST) in this work is defined as the time required to reach within 10% of the demanded steady state value.

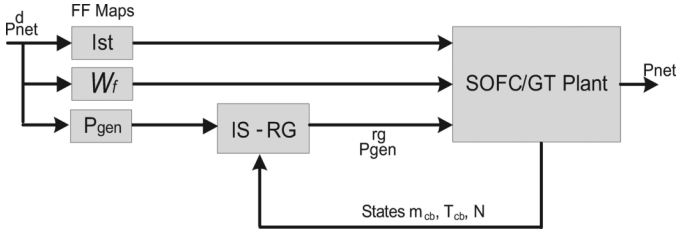

Fig. 5. Schematic of the closed-loop SOFC/GT plant with the IS-RG controller.

A. Conventional Reference Governor for the Hybrid SOFC/GT System

For a dynamic system represented by

$$\dot{x} = f(x, u) \tag{5}$$

subject to constraints

$$(x, u) \in O_f \tag{6}$$

the conventional reference governor is an add-on mechanism used to avoid violation of the constraints [16]. Let u^d be the desired input to the system, the reference governor calculates the optimal feasible input $u = u^{rg}$ according to

$$u^{rg}(t + \delta t) = u^{rg}(t) + K(u^d(t) - u^{rg}(t)) \tag{7}$$

where $K \in [0, 1]$ is determined online by solving the following optimization problem

$$\min_K |u^{rg} - u^d|, \text{ subject to } (x, u^{rg}) \in O_f. \tag{8}$$

This formulation implies that all the constraints are satisfied while the desired reference input is tracked as close as possible.

For the hybrid SOFC-GT system with the feedforward control considered in this study, the external input is the net power demand P^d_{net} and a reference governor is incorporated for the generator command P_{gen}, resulting in the closed-loop system shown in Fig. 5. Note that when the net power demand P^d_{net} steps up, both the fueling rate W_f and current drawn from the SOFC I_{st} will step up according to the feedforward map, while the command to the generator load will be determined by the reference governor to assure system stability.

In the conventional reference governor implementation, the optimization problem (8) subject to the no-shutdown constraint is solved online to determine K. For general nonlinear systems where analytic solutions for the optimization problem are impossible to obtain, this is performed by repeated simulations and 1-D search (note that only one variable K is involved in the optimization). For the SOFC/GT system, the conventional reference governor is implemented by simulating the system model repeatedly for different K in online optimization, using bi-sectional search. A transient scenario with a net power demand step up from 20 to 21 kW is considered and the conventional RG is applied to the full-order model with 55 states. The power response of the system with the reference governor has a settling time of 75 s (a significant improvement from 168 s achieved by the fastest rate limiter), while system shutdown is avoided. However, for a 500-s input profile (the step is applied at 100 s), it took 1800 min on a laptop computer (Pentium 3 GHz, 2 GB RAM) to simulate the system shown in Fig. 5. This computational demand, mainly due to the repeated simulations required for online optimization, renders the controller infeasible for our application.

B. Incremental Step Reference Governor

To develop computationally feasible load conditioning strategies for the hybrid SOFC-GT system, we propose a novel algorithm referred to as the incremental step reference governor (IS-RG). The ingredients of the proposed algorithm that contribute to the computational efficiency include that: 1) the feasibility of the control command is determined based on whether the state vector belongs to the region of attraction of the corresponding stable equilibrium, rather than through simulations and optimization; and 2) a fixed incremental step, rather than a range of input values, is evaluated to determine the permissibility of load increase. Online optimization is not performed.

It is noted that the constraint of no-shutdown for transient operation can be expressed in terms of (6), where

$$O_f = R_A(x^u_{ss}) \tag{9}$$

and $R_A(x^u_{ss})$ denotes the region of attraction of the stable equilibrium point x^u_{ss} corresponding to input u. Here the input u is the output of the reference governor, namely $u^d = P_{\text{gen}}$, $u = P^{rg}_{\text{gen}}$. A formal definition of the region of attraction is given here for completeness.

Definition 6.1 Region of Attraction [17]: Let $x = x^u_{ss}$ be an asymptotically stable equilibrium point for the nonlinear system (5) with input u, where $f : D \to R^n$ is locally Lipschitz and $D \subset R^n$ is a domain containing x^u_{ss}. Let $\phi(t; x)$ be the solution of (5) with the initial state x at time $t = 0$. The region of attraction of the equilibrium, denoted as $R_A(x^u_{ss})$, is defined by

$$R_A(x^u_{ss}) = \left\{ x \,\middle|\, \begin{array}{l} x \in D, \\ \phi(t; x) \text{ is defined } \forall\, t \geq 0, \\ \lim_{t\to\infty} \phi(t; x) = x^u_{ss} \end{array} \right\}. \tag{10}$$

The following definitions are also needed to describe the incremental step reference governor.

Definition 6.2 Permissible Incremental Step (IS) Change: Given a state x_1 and input u, where

$$x_1 \in R_A(x^u_{ss}). \tag{11}$$

If

$$x_1 \in R_A(x^{u+\delta u}_{ss}) \tag{12}$$

then δu is a permissible IS change.

For the SOFC-GT system, if δu is permissible when $x(t) = x_1$, that implies that the generator load can be increased from P^{rd}_{gen} to $P^{rd}_{\text{gen}} + \delta u$. Note that for a given δu, whether it is a permissible IS depends on both the state at the time this step will be attempted and the u (which will determine $x^{u+\delta u}_{ss}$).

A graphic explanation of the permissible incremental step change is shown in Fig. 6. The operating point at time $t = t_1$ belongs to $R_A(x^{u_1}_{ss})$ but not to the $R_A(x^{u_1+\delta u}_{ss})$, thus δu is not a permissible incremental step at $t = t_1$. At time $t = t_2$ the

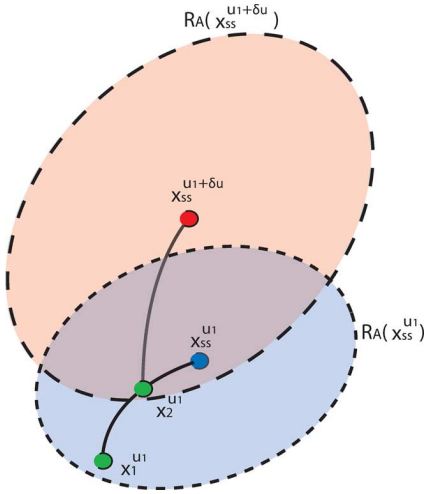

Fig. 6. Schematic explaining the IS-RG principle.

operating point belongs in $R_A(x_{ss}^{u_1+\delta u})$, thus the step change in the input from u_1 to $u_1+\delta u$ is permissible.

Definition 6.3 Incremental Step – Reference Governor: For the dynamic system of the form $\dot{x}(t)=f(x,u)$, given the desired input $u^d(t)$ and $\delta u=\text{constant}$, the IS-RG calculates the input $u(t)$ according to

$$u(t+\delta t) = \begin{cases} \min\left[u(t)+\delta u,\ u^d(t)\right], & \text{if } \delta u \text{ is a permissible } IS \\ \min\left[u(t),\ u^d(t)\right], & \text{if } \delta u \text{ is not a permissible } IS \end{cases} \tag{13}$$

where $u(t+\delta t)$ denotes the input to be applied at the next time step after t.

The IS-RG applies incremental steps to the reference command until the final desired setpoint u^d is reached. To guarantee that the desired setpoint will be reached, i.e.,

$$\lim_{t\to\infty} u(t)=u^d$$

a sufficient condition is that δu is chosen such that

$$x_{ss}^{u_0+k\delta u}\in R_A(x_{ss}^{u_0+(k+1)\delta u}),\ k=0,1,2,\ldots \tag{14}$$

where u_0 is the initial control input. Namely, the equilibrium corresponding to the current input, $u_0+k\delta u$, should belong to the region of attraction corresponding to the equilibrium with $u_0+(k+1)\delta u$. Condition (14) can be satisfied by choosing δu to be sufficiently small. If an intermediate equilibrium, $x_{ss}^{u_i}$ does not belong to the region of attraction of the next equilibrium, we run into the possibility of reaching an intermediate equilibrium where the load cannot be increased any further by the incremental amount specified by δu. It is shown later that a small δu will not slow down the system as long as the sampling time is relatively fast compared to the system dynamics.

The main advantage of the proposed IS-RG is that it converts an optimization problem [i.e., determining K for (8)] into the problem of checking whether δu is a permissible step at each time, or equivalently, whether the state x belongs to $R_A(x_{ss}^{u+\delta u})$, where (x,u) is the current state and the generator load respectively. The latter problem can be solved much more easily if one can find a way to characterize the region of attraction as a function of the input.

For the SOFG/GT system described in this paper, however, the region of attraction corresponding to each input value is characterized by 55 states, and the measurement of all states has to be used online to check whether δu is a permissible step if (13) is implemented as it is. This is neither necessary nor desirable, as we know that some states will not be important in deciding the feasible input step size. In the sequel, we propose to characterize the region of attraction used for IS-RG implementation using a physics-based nonlinear reduced order model and show that only three state measurements are required to describe the R_A of the SOFC/GT system while the remaining 52 states can be neglected.

C. Reduced Order Model and R_A Characterization

In this section, we describe a reduced order model (ROM) that allows us to characterize the region of attraction in a low dimensional space to facilitate the IS-RG implementation. Three important states are the gas mass inside the catalytic burner, the temperature of the catalytic burner and the shaft rotational speed. These states have been identified to be the key states by linearizing the plant at various load operating points, then normalizing the inputs, outputs and states and finally by performing a balanced realization [18]. The resulting balanced realization shows these three states as the dominating ones, separating them from the rest of the states.[4] The selection of these states can also be justified physically given that they define the energy delivered to the turbine and thus they dictate the shaft dynamics. Note that the reduced order model with three states will not capture some characteristics of the full order model, such as the current distribution, the main goal for this ROM is to capture the shutdown dynamics of the full order model (FOM).

The ROM uses mass and energy balance to derive the state equations and the compressor and turbine maps as well as the electro-chemical equilibrium relations to capture the key nonlinear behavior. In order to apply the mass and energy conservation to the SOFC/GT system, the mass and temperature of the reduced order model is revised to be the mass and temperature of the lumped volumes SOFC and CB. The state equations are then given as

$$\begin{aligned} \frac{dm_l}{dt} &= W_c - W_t, \\ m_A c_{P_A}\frac{dT}{dt} &= H_{\text{abs}}^{\text{air in}} + H_{\text{abs}}^{\text{fuel in}} - H_{\text{abs}}^{\text{out}} - U_{st}I_{st}, \\ \frac{dN}{dt} &= \frac{P_t\eta_m - P_c - P_{\text{gen}}}{\alpha N\cdot J} \end{aligned} \tag{15}$$

where m_l, T are the mass and temperature of the lumped SOFC and CB volume, respectively, and N is shaft speed. W_t and W_c are the flows that go through the turbine and compressor, respectively, they are calculated using the turbine and compressor maps shown in Figs. 7 and 8, respectively. Details on the tubine and compressor model can be found in Appendix A. In (15),

[4]It should be noted that the linearization and balanced realization is used only to identify the dominant states. The resulting linearized model is not used for the design or implementation of the IS-RG.

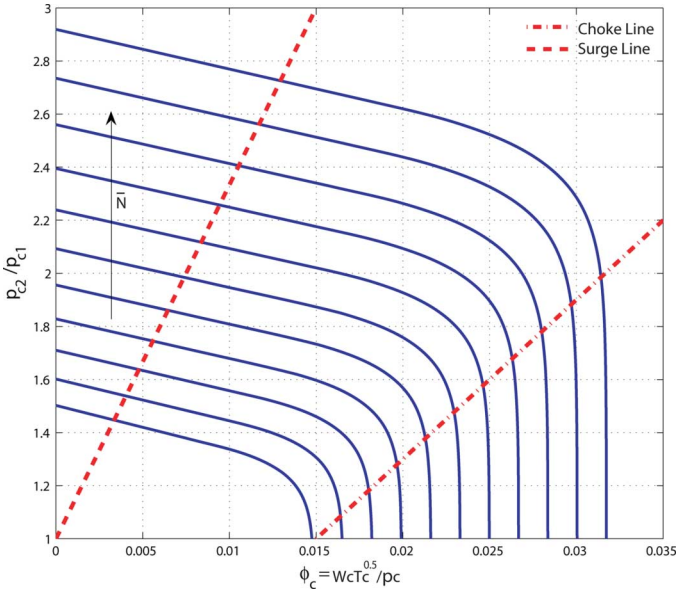

Fig. 7. Compressor map used for both FOM and ROM.

$m_A = 2.84$ kg is the total mass of the SOFC and CB, $c_{P_A} = 500$ J/kg/K is the average heat capacity of all the SOFC solid layers (including the inter-connector and PEN) and $H_{\rm abs}$ is the absolute enthalpy defined as the enthalpy at inlet or outlet temperature, minus the enthalpy at reference temperature ($T_{\rm ref} = 273$ K) plus the enthalpy of formation:

$$H_{\rm abs} = H_T - H_{T_{\rm ref}} + H_f. \tag{16}$$

Note that, $H_{\rm abs}^{\rm air\ in}$ is the absolute enthalpy of the incoming air from the compressor, $H_{\rm abs}^{\rm fuel\ in}$ is the absolute enthalpy of the incoming fuel and $H_{\rm abs}^{\rm out}$ is the sum of the absolute enthalpy of the outlet flow species. Seven species are assumed in the CB outlet flow, namely H_2, N_2, O_2, H_2O, CH_4, CO, CO_2. Furthermore, x_i and $h_{i,\rm abs}^{\rm out}$ are the mole fraction and formation enthalpy of the ith species. Note that x_i is calculated from the FOM as a function of the load $P_{\rm net}$ and implemented in the ROM as look-up tables. An example of such a lookup table for the species CO is given in Fig. 9. Similar maps are integrated for all eight species. This simplification was done based on the results of [11], where it is shown that the reaction kinetics are very fast compared to the temperature dynamics and thus can be ignored.

Furthermore, the pressure in the lumped unit is calculated from the ideal gas law as $pV = nRT$, with p being the pressure, n is the sum of moles in the volume and V is the volume of the SOFC and CB. Finally, U_{st} and I_{st} are the SOFC stack voltage and current respectively and are calculated from the FOM. The stack voltage-current relationship is shown in Fig. 10. Note that Fig. 10 is not the polarization curve of the SOFC stack, for which the partial pressure of reactants and temperature are often held as constant. Instead, Fig. 10 reflects the fact that fuel utilization is changed for different load (current) over the load (current) range according to the optimization results. The fuel utilization as a function of net power is shown in Fig. 11, where fuel utilization is defined as the amount of fuel provided to the SOFC over the amount of fuel that is exiting the SOFC.

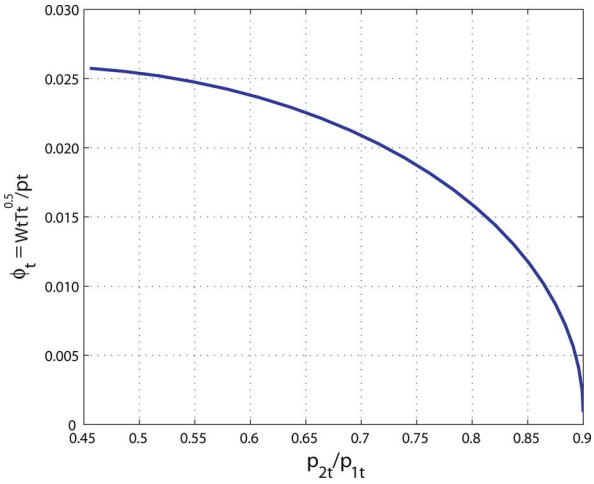

Fig. 8. Turbine map used for both FOM and ROM.

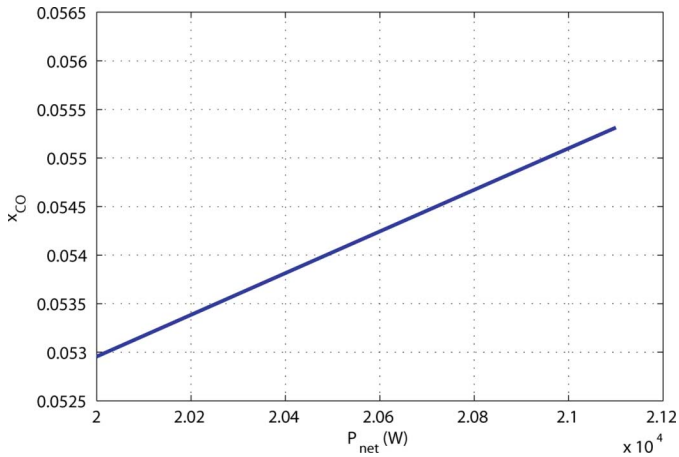

Fig. 9. CO molar fraction in ROM as a function of load.

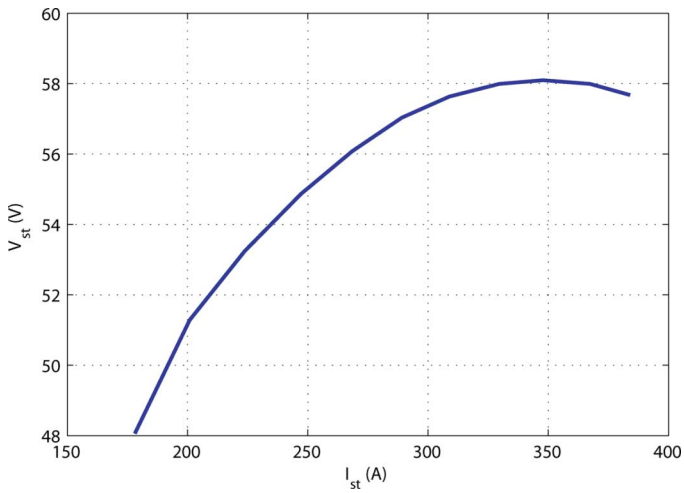

Fig. 10. Stack voltage-current relationship for the SOFC with the feedforward control.

Comparing the response of the FOM and the ROM in terms of the shaft power, the two models match well as shown in Fig. 12. Most importantly, the shutdown effect is captured during a 660 W step as shown in Fig. 12(c). Note that during the period

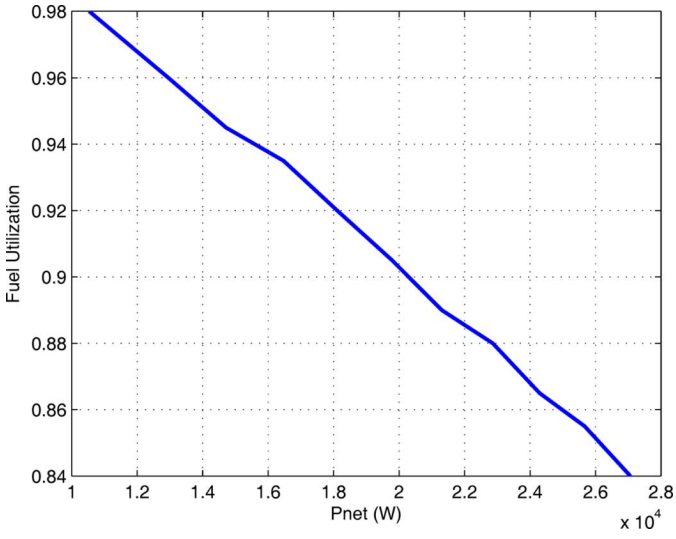

Fig. 11. Fuel utilization for variable net power.

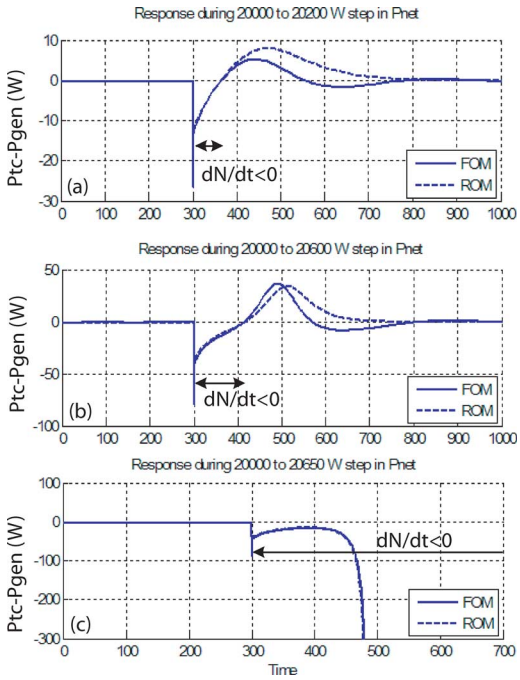

Fig. 12. Comparison of the reduced and full-order model responses to load steps change.

of time when the shutdown can occur (i.e., when $\dot{N} < 0$ or $P_{tc} - P_{\text{gen}} < 0$), the behavior of the FOM and ROM is almost identical as shown in Fig. 12.

Based on the ROM and FOM analysis, we characterize the R_A of the FOM in terms of the dominant states m_{cb}, T_{cb} and N for the range of loads. The remaining states have negligible effect on the R_A, i.e., the 55-dimension R_A can be collapsed into a 3-dimension R_A. This result is also numerically verified for selected load conditions. The R_A plot for $P_{tc} = 20$ kW, together with the corresponding stable equilibrium point, is shown in Fig. 13, where the R_A was calculated numerically given the non-analytic form of the model. The boundary surface shown in Fig. 13(a) divide the 3-D space into two regions, a (T_{cb}, m_{cb}, N) point is considered to be within the region of attraction if it is on the same side as the equilibrium point.

To better assist readers to view the R_A plot, the 2-D plots are also given in Fig. 13(b), with N fixed as a parameter. For each N, the curve on Fig. 13(b) divides the plane into two regions: the upper-right part is within the region of attraction, while the lower-left part is outside.

The boundaries of the R_A [i.e., each of the curves shown in Fig. 13(b)] can be approximated by a linear function of the form

$$T_{cb\,B}^{P_{\text{net}}} = a^{P_{\text{net}}}(N) \cdot m_{cb} + b^{P_{\text{net}}}(N). \tag{17}$$

The parameters $a^{P_{\text{net}}}(N)$ and $b^{P_{\text{net}}}(N)$ are calculated for different shaft speeds at each P_{net} and are stored as lookup tables, indexed by N and P_{net}, for online implementation.

D. Implementation of the IS-RG for the SOFC/GT System

Utilizing the R_A calculated offline and stored for online look up, the IS-RG controller safeguards the system with a minimum online computational requirement. Fig. 14 shows the simulation of the closed loop FOM with IS-RG for a 20 to 21 kW step increase in the desired net power, where δP_{gen} is chosen as 20 W. Note that for the same step, the open-loop system (without the IS-RG) shuts down shortly after the step is applied (dashed line in Fig. 14), while the open loop system with a P_{gen} rate limiter exhibits a settling time of 168 s. The settling time achieved the IS-RG is about 76 s, which is comparable to 75 s achieved by the conventional reference governor, but it represents a significant improvement compared to the rate limiter. The required simulation time for the IS-RG is 145 s compared to the 1800 min for the conventional reference governor for this 500 s run time.

Note that the size of δP_{net} is set to 20 W to ensure that condition (14) is met. Furthermore, note that during a 20 to 20.3 kW step the IS-RG exhibits the same performance as the open-loop plant since the equilibrium for $P_{\text{net}} = 20$ kW belongs in the R_A ($P_{\text{net}} = 20.3$ kW) (see Fig. 15).

It should also be noted that the main function of the IS-RG is to avoid shutdown. This is achieved by slowing down the application of the generator load to ensure safe operation. It does not attempt to change the dynamics of the system. In order to enhance the performance, the IS-RG controller will be combined with a proportional controller that regulates the fuel flow into the CB during a transient to increase the energy input into the turbine, thereby helping sustain the applied load.

E. Effects of the Sampling Period (SP)

Since the incremental step is applied whenever it is deemed feasible by the IS-RG at each sampling instant, the sampling period of the controller will also affect the controller performance and computational requirements for the IS-RG implementation. While fast sample may help improve the power response, it will also increase the computational load. In this subsection, the effects of the sampling period (SP) of the controller on the system performance will be examined to understand the tradeoffs.

In our implementation, the controller is discretized using a sampler in the input (measurements) and a zero-order hold at the output (reference command). The sampling period of the controller, for the simulation results shown in Figs. 14, 15, is equal to 0.01 s (i.e., 100 Hz). Fig. 16 shows the system response

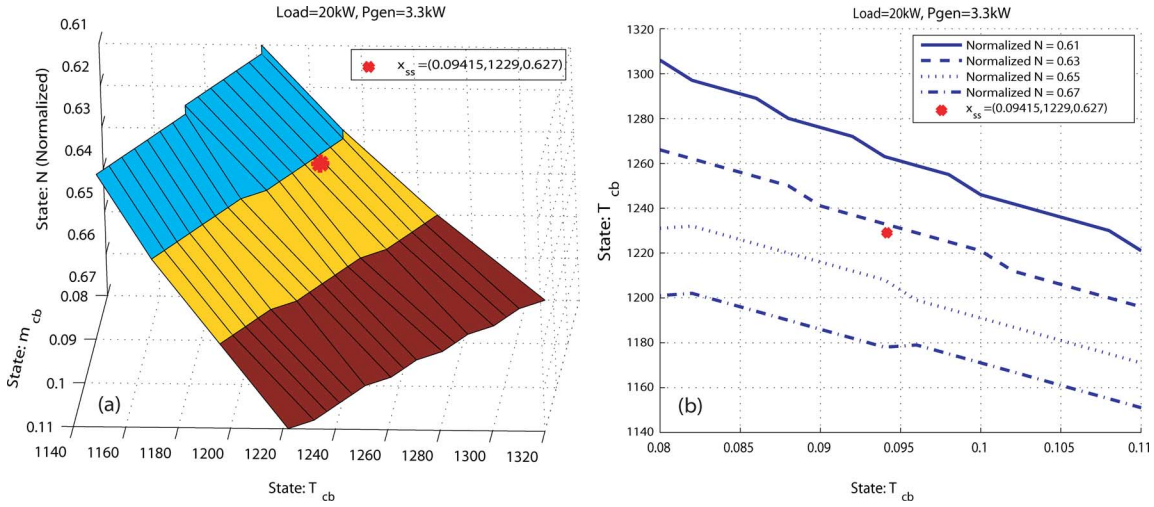

Fig. 13. Boundaries of R_A in 3-D and 2-D plots [(a) and (b), respectively] for $P_{\text{net}} = 20$ kW.

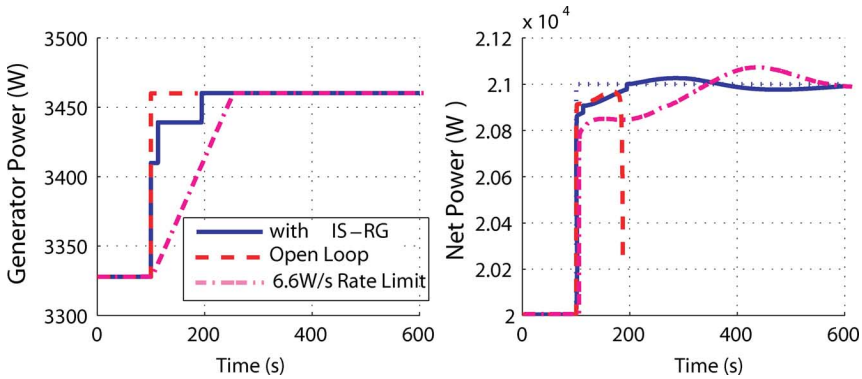

Fig. 14. Open and closed loop (with IS-RG) responses to a load step change from 20 to 21 kW.

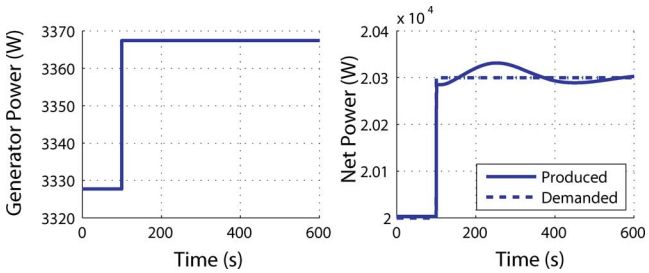

Fig. 15. IS-RG closed loop response to a load step change from 20 to 20.3 kW.

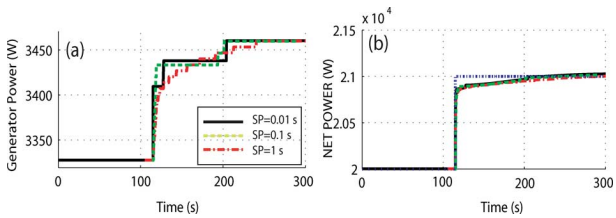

Fig. 16. IS-RG response with various sampling periods (SP).

for a 20 to 21 kW step for 0.01, 0.1, and 1 s sampling periods and $\delta P_{\text{net}} = 20$ W.

It can be seen that for sampling frequencies of 100, 10, and 1 Hz, the system's settling time during a 20 to 21 kW step increase in load is 76, 77, and 83 s, respectively (see also Table I for the summary). This simulation shows that for a 10 times increase in the IS-RF sampling period, the settling time deteriorates by 1%, while for a 100 times increase in sampling period, the settling time deteriorates by 9%. This result confirms that, without requiring high sampling frequency, the IS-RG can achieve the performance at the desired level. Furthermore, reducing the sampling frequency will reduce the computational load. This computational load reduction, however, is not very noticeable in our simulation when the plant and controller are simulated on the same CPU, as summarized in Table I.

TABLE I
COMPARISON OF SETTLING TIMES AND SIMULATION TIMES FOR DIFFERENT OPEN AND CLOSED LOOP SCHEMES RESPONDING TO A LOAD STEP FROM 20 TO 21 kW

Control Type	Settling (s)	Simulation Time (min)
Open Loop	-	2.1
Rate Limiter	168	2.4
IS-RG (1 Hz)	83	2.2
IS-RG (10 Hz)	77	2.2
IS-RG (100 Hz)	76	2.3
IS-RG and P (100 Hz)	61	2.3
Conventional RG (100Hz)	75	1800

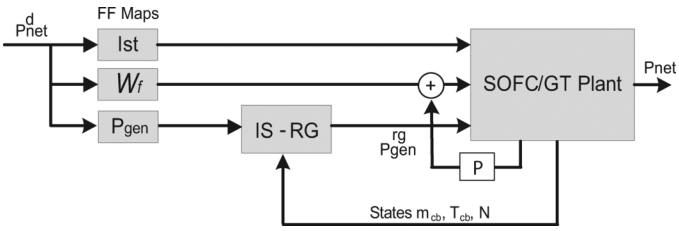

Fig. 17. Control schematic with IS-RG and proportional feedback control.

V. Combining Proportional CB Fuel Controller With IS-RG

The R_A of the SOFC/GT model is shown to be a strong function of the CB temperature and mass (besides the shaft speed). In order to allow for larger and faster load steps we choose to add extra fuel to the system during the transient. The extra fuel will increase the CB temperature and mass flow in order to support the generator load and thus improve the load following performance of the plant. The corresponding control configuration is shown in Fig. 17, where the proportional control is used such that when integrated with the IS-RG, the feedback control signal is zero at the steady state and the equilibriums of the system are not changed.

The extra fuel flow into the system, W_{ef}, is controlled proportionally to the turbine power deficiency, i.e., the desired turbine power P_t^* as a function of the demanded net power minus the current turbine power P_t

$$W_{ef} = K_P\left(P_t^*(P_{\rm net}) - P_t\right) \tag{18}$$

where $P_t^*(P_{\rm net})$ is the desired turbine power as a function of the net power. Note that the turbine power cannot be directly measured, we use the measurement of the CB pressure and temperatures to estimate the turbine power. Since IS-RG already utilizes these measurements for its implementation, no additional measurements are required for the P controller.

The incorporation of the P controller will affect the region of attraction of the system. The region of attraction with the proportional controller is shown in Fig. 18. Compared to Fig. 13, one can see that all curves in Fig. 18 are moved downwards, which implies that the region of attraction (the upper-right region above the curves) is expanded.

The system response with the IS-RG and the proportional controller that adds extra fuel in the SOFC is shown in Fig. 19. The overshoot of the fuel allows for larger and faster $P_{\rm gen}$ steps, contributing to improved load following capabilities with a 61 s settling time for a 20 to 21 kW step in load, as compared to 76 s achieved without the P controller. Increasing further the value of the proportional gain K_P will increase the response speed even more, but it will also increase the temperature gradient in the CB. The results with all the control schemes and associated computational cost (as measured by the simulation time) are summarized in Table I, with a reference being made to the rate limited control.

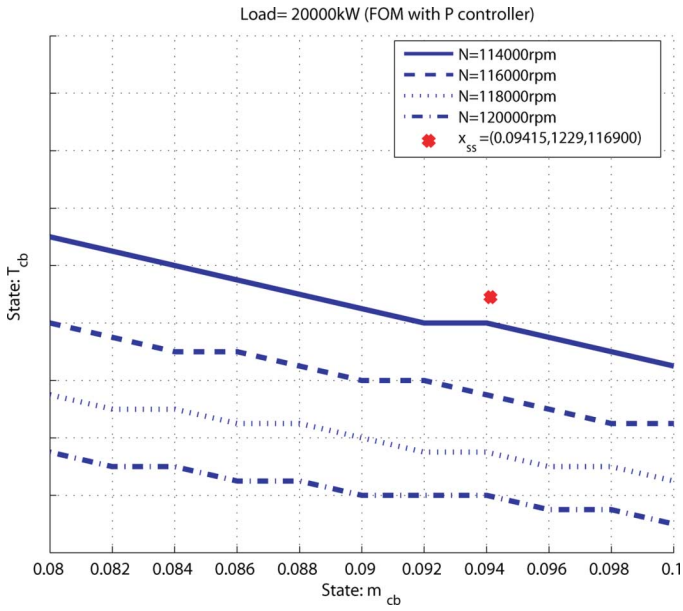

Fig. 18. Boundaries of the region of attraction for the system with the CB fuel proportional controller, $P_{\rm net} = 20$ kW.

VI. Summary and Conclusion

In this paper, the efficiency and the transient operation of a hybrid SOFC and GT system are analyzed. A nonlinear, control oriented model is developed and used initially for defining, via optimization, the fuel, current, and generator load setpoints that yield the highest system efficiency. However, utilizing these setpoints for load transitions is shown to cause system shutdown when large and fast transitions are attempted. The shutdown phenomenon is analyzed and the coupling dynamics between the fuel cell and the gas turbine are identified as the main cause for the shutdown phenomenon.

To mitigate the shutdown problems associated with the open-loop operation, an IS-RG control scheme is developed and implemented to modify the application of the generator load. Slowing down the application of the generator load allows more power delivered to the shaft during transients, thereby preventing a large rotational speed drop of the shaft. The IS-RG achieves the constraint enforcement without compromising tracking performance and without using online optimization.

Appendix

For a complete description of the reduced-order model used in the IS-RG design and implementation, we list all the equations needed to represent the compressor and turbine model in this Appendix. A summary of all the turbine and compressor variables is given in Fig. 20 with their corresponding placement.

Compressor Model: Neglecting heat losses, the power required to drive the compressor (P_c) can be related to the mass flow rate through the compressor, W_c, and the total enthalpy change across the compressor from the first law of thermodynamics as

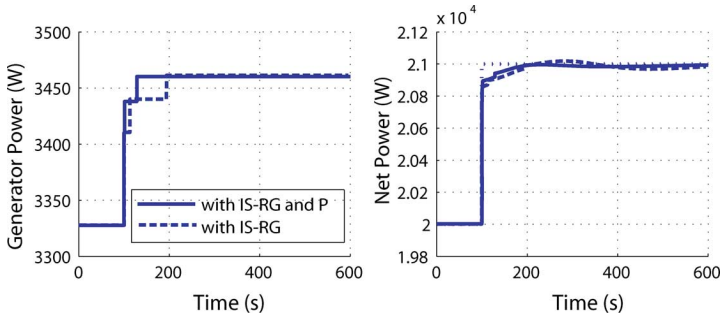

Fig. 19. Response to a step from 20 to 21 kW with IS-RG and P control of fuel in CB.

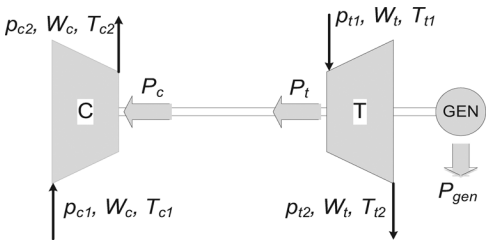

Fig. 20. Compressor, turbine, shaft, and generator schematic.

$$P_c = W_c(h_{c2} - h_{c1}) \tag{19}$$

where h_{c1} and h_{c2} are the enthalpy of the inlet and the outlet flow, respectively. Assuming that the specific heat coefficients of air do not change and by introducing the compressor isentropic efficiency, η_c, we have

$$T_{c2} = T_{c1} \cdot \left(1 + \frac{1}{\eta_c}\left(\left(\frac{p_{c2}}{p_{c1}}\right)^{(\gamma-1)/\gamma} - 1\right)\right) \tag{20}$$

$$P_c = W_c c_p^{\text{air}} T_{c1} \frac{1}{\eta_c}\left(\left(\frac{p_{c2}}{p_{c1}}\right)^{(\gamma-1)/\gamma} - 1\right). \tag{21}$$

Typically, the relation between compressor flow and efficiency to pressure ratio and compressor speed is specified in terms of nondimensional mass flow rate parameter, ϕ_c, and compressor rotational speed parameter, $\bar{N}_c$, that are defined as

$$\phi_c = \frac{W_c\sqrt{T_{c1}}}{p_{c1}} \tag{22}$$

$$\bar{N}_c = \frac{N}{\sqrt{T_{c1}}}. \tag{23}$$

Details on the polynomial approximation of the compressor map can be found in [2].

Turbine Model: The turbine is powered by the energy of the exhaust gas. The power input to the turbine P_t can be obtained from the first law of thermodynamics, neglecting the heat transfer, as

$$P_t = W_t(h_{t1} - h_{t2}) \tag{24}$$

where h_{t1} and h_{t2} are the enthalpy of the inlet and the outlet turbine flow respectively. For a given pressure ratio across the turbine, the outlet temperature can be computed assuming isentropic expansion

$$\left(\frac{T_{t1}}{T_{t2,is}}\right) = \left(\frac{p_{t1}}{p_{t2}}\right)^{(\gamma-1)/\gamma} \tag{25}$$

where $T_{t2,is}$ is the temperature of the exhaust gas leaving the turbine if the expansion were isentropic. The turbine isentropic efficiency, η_t, is introduced to calculate the turbine outlet temperature and power

$$T_{t2} = T_{t1}\left(1 - \eta_t\left(1 - \left(\frac{p_{t2}}{p_{t1}}\right)^{(\gamma-1)/\gamma}\right)\right) \tag{26}$$

$$P_t = W_t c_p T_{t1} \eta_t \left(1 - \left(\frac{p_{t2}}{p_{t1}}\right)^{(\gamma-1)/\gamma}\right). \tag{27}$$

The flow through the turbine is given as

$$W_t = \frac{A_{\text{eff}} p_{t2}}{T_{t2}}\left(\left(\frac{p_{t1}}{p_{t2}} - g + 1\right)^{2/\gamma} - \left(\frac{p_{t1}}{p_{t2}} - g + 1\right)^{(\gamma+1)/\gamma}\right)^{0.5} \tag{28}$$

where $A_{\text{eff}} = 0.07$ m^2 is the effective flow area and $g = 0.9$ is the pressure ratio where the flow becomes zero. The isentropic efficiency is then given as a function of the blade-speed ratio U/C, defined as

$$\frac{U}{C} = \frac{\pi D N}{\sqrt{2c_p T_{t1}\left(1 - \left(\frac{p_{t2}}{p_{t1}}\right)^{(\gamma-1)/\gamma}\right)}} \tag{29}$$

where D denotes the turbine blade diameter.

REFERENCES

[1] H. Xi, "Dynamic modeling and control of planar SOFC power systems," Ph.D. dissertation, Dept. Naval Arch. Marine Eng., Univ. Michigan, Ann Arbor, 2007.

[2] V. Tsourapas, "Control analysis of integrated fuel cell systems with energy recuperation devices," Ph.D. dissertation, Dept. Naval Arch. Marine Eng., Univ. Michigan, Ann Arbor, 2007.

[3] P. Kuchonthara, S. Bhattacharya, and A. Tsutsumi, "Energy recuperation in solid oxide fuel cell (SOFC) and gas turbine (GT) combined system," *J. Power Sources*, vol. 117, pp. 7–13, 2003.
[4] S. Kimijima and N. Kasagi, "Cycle analysis of micro gas turbine molten carbonate fuel cell hybrid system," *JSME Int. J.*, vol. 48, pp. 65–74, 2005.
[5] A. M. Murshed, B. Huang, and K. Nandakumar, "Control relevant modeling of planer solid oxide fuel cell system," *J. Power Sources*, vol. 163, pp. 830–845, 2007.
[6] X. Wang, B. Huang, and T. Chen, "Data-driven predictive control for solid oxide fuel cells," *J. Process Control*, vol. 17, pp. 103–114, 2007.
[7] A. Vahidi, A. Stefanopoulou, and H. Peng, "Model predictive control for starvation prevention in a hybrid fuel cell system," in *Proc. Amer. Control Conf.*, 2004, pp. 834–839.
[8] R. A. Roberts and J. Brouwer, "Dynamic simulation of a pressurized 220 kw solid oxide fuel-cell gas-turbine hybrid system: Modeled performance compared to measured results," *J. Power Sources*, vol. 3, pp. 18–25, 2006.
[9] C. Wchter, R. Lunderstädt, and F. Joos, "Dynamic model of a pressurized SOFC/gas turbine hybrid power plant for the development of control concepts," *J. Fuel Cell Sci. Technol.*, vol. 3, pp. 271–279, 2006.
[10] C. Stiller, B. Thorud, O. Bolland, R. Kandepu, and L. Imsland, "Control strategy for a solid oxide fuel cell and gas turbine hybrid system," *J. Power Sources*, vol. 158, pp. 303–315, 2006.
[11] H. Xi, J. Sun, and V. Tsourapas, "A control oriented low order dynamic model for planar SOFC using minimum gibbs free energy method," *J. Power Sources*, vol. 165, pp. 253–266, 2007.
[12] V. Tsourapas, J. Sun, and A. Nickens, "Control oriented modeling and analysis of a hybrid solid oxide fuel cell and gas turbine (SOFC/GT) system," in *Proc. ASME Conf. Fuel Cell Sci. Technol.*, 2007, p. FC-07-1086.
[13] V. Tsourapas, J. Sun, and A. Stefanopoulou, "Modeling and dynamics of a fuel cell combined heat power system for marine applications," *IASME Trans.*, vol. 2, no. 1, pp. 287–293, 2004.
[14] V. Tsourapas, J. Sun, and A. Stefanopoulou, "Dynamics, optimization and control of a fuel cell based combined heat power (chp) system for shipboard applications," in *Amer. Control Conf.*, 2005, pp. 1993–1998.
[15] J. Sun and I. Kolmanovsky, "A robust load governor for fuel cell oxygen starvation protection," *IEEE Trans. Control Syst. Technol.*, vol. 13, no. 6, pp. 911–920, Nov. 2005.
[16] I. V. K. E. Gilbert and K. T. Tan, *Int. J. Robust Nonlinear Control*, vol. 5, pp. 6487–504, 1995.
[17] H. Khalil, *Nonlinear Systems*, 3rd ed. Englewood Cliffs, NJ: Prentice-Hall, 2002.
[18] J. Freudenberg, *A First Graduate Course in Feedback Control*. Ann Arbor: University of Michigan, 2002, EECS 565 Coursepack.

Vasilis Tsourapas received the M.S. degree in naval architecture and marine engineering from the National Technical University of Athens, Athens, Greece, in 2003, the M.S. degree in mechanical engineering and the Ph.D. degree in Naval Architecture and Marine Engineering focusing on optimization and control analysis of fuel cell power systems from the University of Michigan, Ann Arbor, in 2005 and 2007, respectively.

He currently holds the position of Lead Engineer with the Innovation Center of Eaton Corporation, Southfield, MI.

Dr. Tsourapas was a recipient of the "Department of Defense" Graduate Fellowship and his Ph.D. research was funded by the Office of Naval Research (ONR), the National Science Foundation (NSF), the Automotive Research Center (ARC) of the University of Michigan, and the U.S. Army.

Jing Sun (S'87–M'89–SM'00–F'04) received the Ph.D. degree from University of Southern California, Los Angeles, in 1989, and the B.S. and M.S. degrees from University of Science and Technology of China, Beijing, China, in 1982 and 1984, respectively.

From 1989–1993, she was an Assistant Professor with the Electrical and Computer Engineering Department, Wayne State University. She joined Ford Research Laboratory in 1993, where she worked in the Powertrain Control Systems Department. After spending almost 10 years in industry, she came back to academia and joined the faculty of the College of Engineering at University of Michigan, Ann Arbor, in 2003 as an Associate Professor. Her research interests include system and control theory and its applications to marine and automotive propulsion systems. She holds over 30 U.S. patents and has coauthored a textbook on robust adaptive control.

Dr. Sun was a recipient of the 2003 IEEE Control System Technology Award.

Anna G. Stefanopoulou received the Diploma from the National Technical University of Athens, Athens, Greece, in 1991, the M.S. degree in naval architecture and marine engineering and the Ph.D. degree in electrical engineering and computer science from the University of Michigan, Ann Arbor, in 1992 and 1996, respectively.

She is presently a Professor with the Mechanical Engineering Department, University of Michigan. She was an Assistant Professor (1998–2000) at the University of California, Santa Barbara, and a Technical Specialist (1996–1997) at the Scientific Research Laboratories at Ford Motor Company. Her current research interests include control of advanced internal combustion engines and fuel cell power systems.